

Crystal structure of the bacterial membrane protein TolC central to multidrug efflux and protein export

Vassilis Koronakis*†, Andrew Sharff†‡, Eva Koronakis*, Ben Luisi‡ & Colin Hughes*

* Department of Pathology, University of Cambridge, Tennis Court Road, Cambridge CB2 1QP, UK

‡ Crystallography & Biocomputing Unit, Department of Biochemistry, University of Cambridge, 80 Tennis Court Road, Cambridge CB2 1GA, UK

† These authors contributed equally to this work

Diverse molecules, from small antibacterial drugs to large protein toxins, are exported directly across both cell membranes of Gram-negative bacteria. This export is brought about by the reversible interaction of substrate-specific inner-membrane proteins with an outer-membrane protein of the TolC family, thus bypassing the intervening periplasm. Here we report the 2.1-Å crystal structure of TolC from *Escherichia coli*, revealing a distinctive and previously unknown fold. Three TolC protomers assemble to form a continuous, solvent-accessible conduit—a ‘channel-tunnel’ over 140 Å long that spans both the outer membrane and periplasmic space. The periplasmic or proximal end of the tunnel is sealed by sets of coiled helices. We suggest these could be untwisted by an allosteric mechanism, mediated by protein–protein interactions, to open the tunnel. The structure provides an explanation of how the cell cytosol is connected to the external environment during export, and suggests a general mechanism for the action of bacterial efflux pumps.

Export of a wide range of molecules across the cell envelope of Gram-negative bacteria is achieved in a single, energy-coupled step, resulting in direct passage across both inner and outer cell membranes and the intervening periplasmic space. The underlying mechanism is determined by the direct interaction of an inner membrane translocase of two proteins, which provides substrate

specificity and energy, with a third in the outer membrane—a protein of the TolC family^{1,2}. When engaged by its export substrate, the translocase recruits TolC to form the active export complex containing all three proteins and the substrate¹. This assembly is transient: when the substrate has been exported, the machinery disengages and the components revert to their separate inner and

Table 1 Summary of data collection and refinement statistics

Compound	Native	Mercury	Oxidized SeMet	
Space group	<i>R</i> 3	<i>R</i> 3	<i>R</i> 3	<i>R</i> 3
Unit cell <i>a</i> (Å)	265.50	262.56	265.11	265.05
<i>c</i> (Å)	95.50	95.53	96.00	95.96
Beamline	SRS 9.6	ESRF BM14	ESRF BM14	APS ID19
Temperature (K)	100	100	100	100
No. of crystals used	1	1	1	1
Wavelength (Å)	0.8700	0.9793	0.9788	0.9790
Max. resolution (Å)	2.50	4.00	2.95	2.95
Unique reflections	86838	18509	52877	52902
Completeness (%)	99.9	98.9	99.9	99.9
Redundancy	9.0	4.0	5.7	4.6
<i>I</i> / <i>σ</i> ²	5.1 (2.3)	8.0 (4.7)	4.5 (4.2)	4.1 (4.2)
<i>R</i> _{sym} (%) [†]	8.8 (18.5)	6.2 (12.2)	7.3 (13.4)	7.1 (13.9)
<i>R</i> _{ano} (%) [†]		6.3 (8.7)	5.7 (7.4)	5.7 (8.7)
Anomalous phasing power		1.46‡	1.1	2.1
<i>R</i> _{culis iso/ano} §		0.95/0.95 [¶]	−/0.91	0.57/0.73
Figure of merit				0.57/0.86
After SHARP refinement		0.156‡		0.450
After solvent flattening		0.586‡		0.840
Refinement				
Resolution range				20.0–2.1
<i>R</i> factor (%)				20.8
<i>R</i> _{free} (%) [¶]				25.7
Ordered water molecules				1,508
R.m.s. deviation from ideal geometry				
Bond lengths (Å)				0.018
Bond angles (°)				1.3
Average <i>B</i> factor (Å ²)				49.88
R.m.s. deviation of monomers (Å)				0.18 ± 0.02

* Figures in parentheses indicate values in the last resolution shell.

† $R_{sym} = \sum |I_{avg} - I|/I_{avg}$, and $R_{ano} = \sum |I_{+} - I_{-}|/I_{+} + I_{-}$.

‡ Data only used to 5.0 Å resolution.

§ $R_{culis} = \sum ||F_{PH} \pm F_P| - F_H(\text{calc})| / \sum |F_{PH}|$.

¶ $||R = \sum |F_{obs} - F_{calc}| / \sum F_{obs} \times R_{free}$ is calculated from about 5% of randomly chosen reflections, which are not used in refinement.

outer membrane resting states¹. This ‘shuttle’ mechanism does not generate periplasmic export intermediates and is fundamentally distinct from processes that determine step-wise translocation across two membranes^{3–5}. TolC and its homologues interact with different translocase complexes, depending on the transport substrate, so that combinatorial assembly provides functional diversity. This system exports large proteins (type I secretion), including enzymes and toxins such as cyclolysin (relative molecular mass, M_r , 170,000)^{1,2,6–8}, and small noxious agents, such as detergents, solvents, heavy metals and antibiotics (multidrug efflux)^{2,9,10}. TolC is therefore an important component in the determination of both pathogenicity and multidrug resistance, and loss of TolC or one of its homologues reduces bacterial survival and attenuates virulence¹¹. This suggests that these proteins may be potential chemotherapeutic targets.

Biochemical and electron microscopy studies have shown that TolC is a trimeric outer membrane protein¹², but a simple porin-like model would not readily suggest a means for interaction with the inner membrane translocase during transport. The detailed three-dimensional structure of TolC that we present here provides insights into the protein’s function and the mechanism of export. It reveals a new architectural design, the α -helical barrel, which forms a tunnel through the periplasm, anchored by a contiguous outer membrane β -barrel. A stereochemical model is proposed for the opening of this structure.

Structure determination

The mature 471-residue TolC protein was detergent-extracted from

E. coli membranes and purified to homogeneity. To obtain crystals, it was necessary to treat TolC with V8 protease, which removed the carboxy-terminal 43 residues. Subsequent assays showed that truncation does not affect function (E.K., unpublished data). Crystals of the protease-truncated TolC grew in space group $R3$ with cell dimensions $a = b = 265 \text{ \AA}$, $c = 95 \text{ \AA}$, $\alpha = \beta = 90^\circ$, $\gamma = 120^\circ$ (in the hexagonal setting). In preparation for data collection, crystals were frozen at 100 K after cryoprotection. The structure was solved by multiple wavelength anomalous dispersion (MAD) using oxidized selenomethionine (SeMet) derivatives¹³.

Data extending to 3.0 \AA and 2.1 \AA were collected from separate crystals around the Se K absorption edge, and these were used to solve and refine the structure. Data were also collected from crystals of native (non-derivatized) protein, without oxidation, at 2.5 \AA , and a model was refined against these data. Comparison of the native and oxidized SeMet models indicates no significant structural differences. The crystals contain one trimer of M_r 141K in the asymmetric unit and have a solvent content of 70%, which is high for protein crystals. The final model has been refined at 2.1 \AA with an R factor of 21% and R_{free} of 25%. The diffraction data quality and refinement statistics are summarized in Table 1 (see Supplementary Information).

Overall architecture

TolC is assembled as a trimer of 428-residue protomers (Fig. 1a). The appearance of the trimer is that of a cannon, with a long axis measuring 140 \AA . For nearly 100 \AA the body forms a uniform cylinder of about 35 \AA internal diameter, in rough agreement with

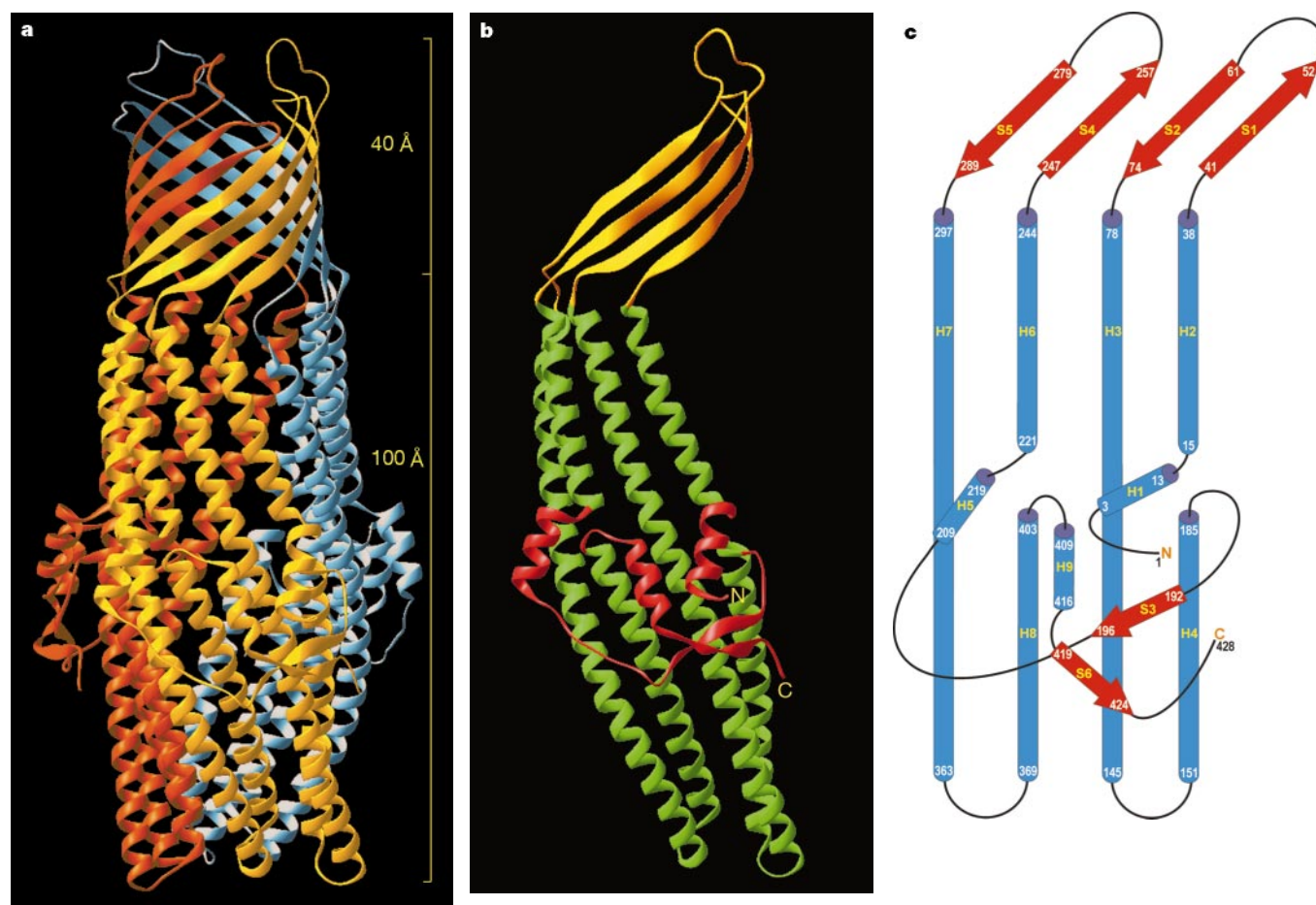


Figure 1 The overall architecture of TolC. **a**, C α trace of TolC. The protomers are individually coloured. The molecular threefold axis is aligned vertically, normal to the plane of the outer membrane. The β -barrel is at the top (distal) end, and the α -helical domain is at the bottom (proximal) end. Figure generated with RIBBONS³⁹. **b**, C α trace of a single

protomer. The β -barrel domain is yellow, the α -helical barrel domain is green and the equatorial domain is red. **c**, Topology diagram of the protomer. Secondary-structure elements are indicated: helices (H) in blue, strands (S) in red. The structural repeat comprises the sets (H1, H2, S1, S2, H3, H4) and (H5, H6, S4, S5, H7, H8).

previous electron microscopy studies¹². The distal (upper) end of the structure is open (see Supplementary Information) and provides a wide solvent access while the proximal (lower) end is tapered to a virtual close. This explains the previous observation that although TolC forms an ion-permeable channel when reconstituted into lipid bilayers, its conductance is unusually low¹⁴. The body has a large interior cavity that is mostly solvent-filled with a volume of roughly 43,000 Å³, making it one of the largest known in a protein structure.

The TolC molecule can be partitioned into a β-domain, an α-helical domain, and a mixed α/β-domain (Fig. 1b). The peptide chain of each protomer weaves up and down the long axis four times, and passes from β-strands (S1, S2, S4, S5), at the distal end of the structure, into α-helices, two of which (H3 and H7) extend to the proximal end (Fig. 1c). The α/β-domain, which we will refer to as the equatorial domain, is made up of strands S3 and S6 and helices H1, H5 and H9 and forms a ‘strap’ around the mid-section of the helical barrel.

In the trimer, the strands of the β-domain associate in an antiparallel orientation to form a 12-stranded β-barrel that is right-twisted (that is, the strands have a positive inclination with respect to the molecular threefold axis). The α-helices forming the main body of the structure also form a 12-stranded antiparallel

barrel, but in contrast to the β-barrel, this α-helical barrel is left-twisted. The opposite twist of the two supersecondary elements originates from the propensity of β-sheets to twist and curve clockwise in globular proteins and of coiled-coil helices to supercoil anticlockwise (for certain sequence repeat patterns¹⁵). The transitions from right-twisted β-barrel into left-twisted α-helical barrel are accommodated through abrupt turns in proline-containing interdomain linkers. The importance of these prolines is underscored by their conservation in the family of bacterial outer membrane efflux proteins. The α-helical barrel is constructed from two types of helix. Long helices (H3 and H7), comprising 67 residues, traverse the entire length from the lower end of the β-barrel to the proximal end of the molecule. The second type are shorter helices of 23 (H2 and H6) and 34 (H4 and H8) residues, respectively. The pairs of the shorter helices stack end to end to form pseudocontinuous helices (H2 and H4; H6 and H8) that, like the long helices, traverse the length of the helical barrel. The equatorial domain is connected to the helical barrel at the junction of these short helices.

The TolC structure comprises an approximate structural repeat (H1–H2–S1–S2–H3–H4 and H5–H6–S4–S5–H7–H8), which is evident in the schematic representation of the protomer (Fig. 1c). The structural repeat corresponds to a repeat in the primary

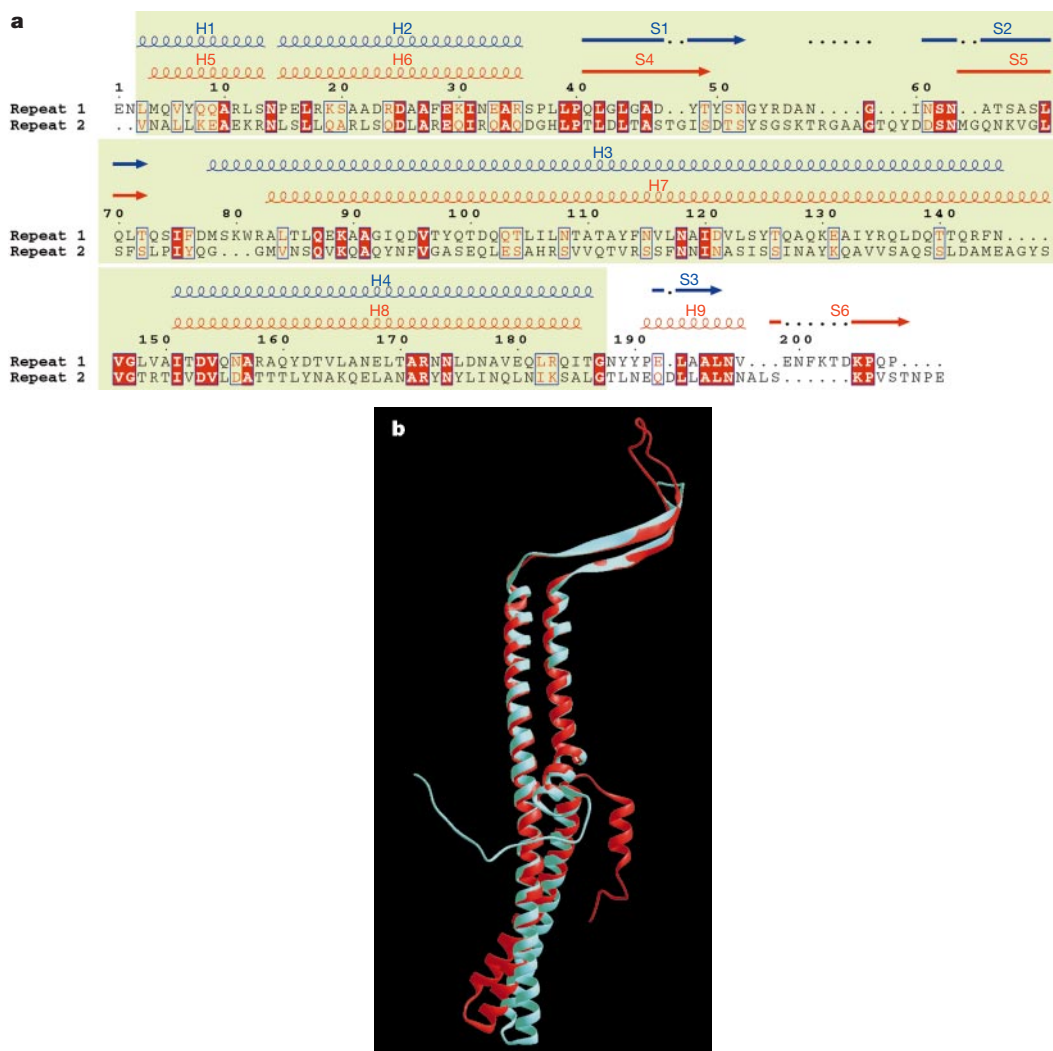


Figure 2 Structural repeat in TolC. **a**, Amino-acid sequence of TolC, annotated with the elements of secondary structure. The sequence has been internally aligned to highlight the structural repeat (shaded in light green). The secondary structure for the N-terminal

repeat is coloured in blue, the C-terminal repeat in red. **b**, Superimposed Cα trace of the structural repeats. Repeat 1 is shown in blue, repeat 2 in red.

sequence (Fig. 2a, b), previously noted in the family of bacterial outer membrane efflux proteins¹⁶. These observations suggest that TolC and its relatives evolved by gene duplication from a common ancestor, which may have functioned as a hexamer.

The β -barrel domain

To date, all of the bacterial outer membrane proteins (OMPs) that have been characterized structurally are β -barrels of 8 to 22 strands, which are inserted in the membrane^{17–24}. As noted in these OMPs, aromatic residues, particularly tyrosine and phenylalanine, cluster in a ring around the base of the TolC β -barrel, delimiting the position of the inner edge of the lipid bilayer²⁵. This clearly indicates that the β -barrel of TolC is similarly located in the outer membrane. The β -barrel of TolC is assembled from three protomers, with each protomer contributing four β -strands. This is so far unique among bacterial OMPs, whose barrels are typically formed from a single monomer. Each of the strands have between 10 and 13 residues, which is common in OMPs. The β -strands must both curve and twist to attain their superhelical path, a movement analogous to the right-handed twisting motion usually associated with the strands in β -sheets in globular proteins. To accommodate the curvature, small or unbranched side chains tend to lie periodically on the inside of the barrel, where they allow the required close packing. Out of phase with the interior repeats, bulkier, β -branched residues lie on the outside of the barrel, where they accommodate the gaps caused by the curving peptide trajectory.

The interiors of the OMPs are often partially or completely occluded^{17,22–25}. In contrast, the β -barrel of TolC is wide open and fully accessible to solvent. The loops at the top end of the β -strands of TolC may close over the mouth as a partial external ‘lid’, but they have comparatively high atomic displacement parameters, indicating that they probably have conformational mobility.

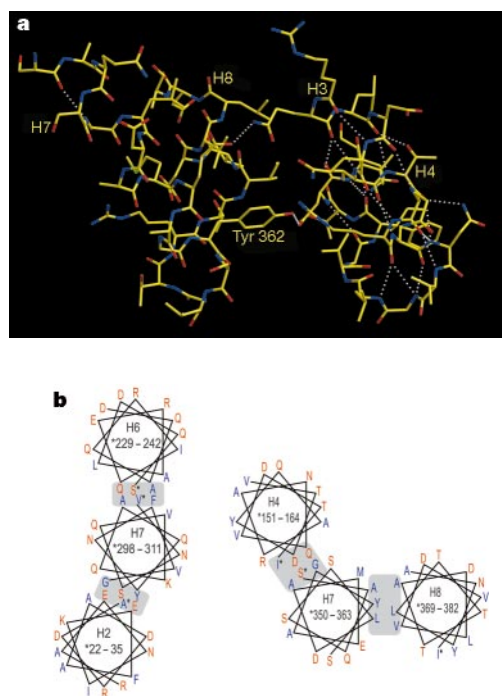


Figure 3 Interfacial contacts in the α -helical barrel. **a**, View of selected contacts in the interface between H3/H4 and H7/H8. The contact made by Tyr 362 is well conserved in the TolC family. We propose that this contact is broken in the open state of the channel. **b**, Helical wheel representations summarizing the interhelical contacts in different parts of the α -helical barrel. The register of lateral contacts between neighbouring helices at the top end of the helical barrel (left) can be maintained in a superhelix, whereas those at the proximal end, between sets of coiled coils (right), can only occur locally. Asterisks indicate the N-terminal residue of each helical segment.

The α -helical domain and coiled-coil interactions

The α -helical barrel is contiguous with the β -barrel and extends into the periplasm. This structure has not been observed before, and it has distinctive features. The upper section of the helical domain (near the β -barrel) is virtually uniform in diameter, and the helices are inclined by -20° relative to the molecular threefold axis. It may not be readily apparent that these helices are coiled coils, but, because they follow an inclined trajectory on the surface of a regular cylinder, they must both curve and twist in space. The TolC helices have a left-handed superhelical twist throughout the entire α -helical barrel, but tend to untwist at the distal end compared with conventional coiled coils. There are no abrupt kinks or bends in either of the long helices, and the continuous change in superhelical trajectory is distributed in small deviations in the local helical twist, as found in other coiled coils²⁶.

The trajectories of the long helices (H3 and H7) remain uniform preceding the equatorial domain, but depart from the cylindrical surface thereafter to form the taper at the proximal end (Fig. 1b). Here, an inner pair of helices (H7 and H8) form a conventional antiparallel coiled-coil. In contrast, an outer pair (H3 and H4) comprise a straight helix (H3) around which its partner (H4) is coiling. The coiled coils also contact each other (Fig. 3a). Given the sequence similarity of the inner and outer pairs of helices, it is striking that they pack so differently when they could pack in a quasi-equivalent manner. This point may have some bearing on the mechanism of channel opening.

Coiled coils are stabilized by an intermeshing of side chains that is commonly referred to as ‘knobs-into-holes’ packing²⁷. A small aliphatic side chain of one helix fits into a small concavity formed by a ring of four small side chains on the second helix. Small non-polar side chains repeat with a characteristic pattern (a-b-c-d-e-f-g) where residues at positions a and d lie in the hydrophobic core of the helical interface. In TolC, the helices at the distal end of the barrel pack laterally with two neighbours and so form two separate interfaces (Fig. 3b). This means that each helix must have two

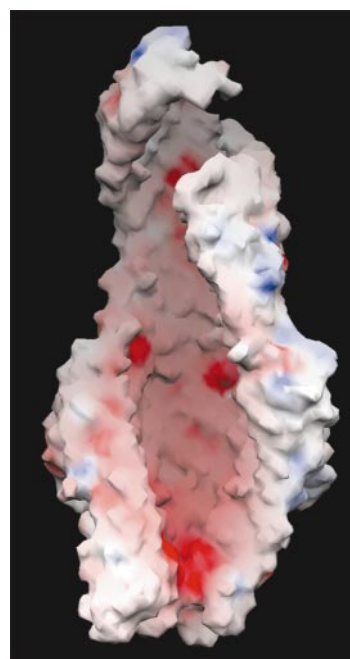


Figure 4 Surface representation of the TolC interior, illustrating the charge distribution. One protomer has been removed to expose the interior view. Charges are shown in red for electronegative and blue for electropositive; white is nonpolar. Figure generated with GRASP⁴⁰.

separate repeats that are out of phase by roughly half a helical turn so that they lie on different exposed faces. There is therefore an approximate equivalence between positions a and c and between d and f. In conventional coiled coils, the register of interfaces is achieved through superhelical twist, but in TolC the superhelical twist is smaller, with the result that the helices can lie on a cylindrical surface. A noteworthy feature of the cylindrical portion of the barrel is that bulkier side chains tend to lie on the exterior face of the barrel, and their steric bulk might accommodate the curvature of the barrel.

The equatorial domain

Unlike other parts of the TolC structure, the equatorial domain has no pseudosymmetry. The helices and strands of this mixed α/β structure pack against the helices of the helical barrel, and its fold is consolidated through numerous hydrogen bonds and van der Waals contacts between side chains. The C-terminal 43 residues that were proteolytically removed to prepare the crystals would extend from the equatorial domain.

Properties of the exposed surfaces

The exterior of the β -barrel is in direct contact with the aliphatic chains of the lipid bilayer in the outer membrane and is largely nonpolar, as expected. The α -helical barrel and equatorial domains present a mixture of predominately nonpolar and isolated electro-

negative and electropositive patches. The surface of the interior cavity from the top of the structure down to the equatorial domain is also predominately nonpolar. On moving toward the proximal end of the α -helical barrel, however, the interior surface becomes increasingly electronegative (Fig. 4). This may have implications for the transport mechanism, as all substrates entering the TolC tunnel will encounter this striking electronegative surface. TolC and its homologues transport molecules with a wide variation in charge. It follows that a pulse of cations early in transport might favour entry of acidic and hydrophobic substrates into the tunnel, whereas a late pulse might catalyse the release of basic molecules.

A proposal for the transport mechanism

TolC is central to the export of diverse compounds, from small molecules to large proteins, in each case interacting with a specific inner membrane translocase. It is apparent that during transport, the tapered proximal end of the trimer must open and, in the case of proteins, the transport substrate must be at least partially unfolded. The simplest opening mechanism envisages that the inner pair of coiled coils rotates around its neighbouring partner to dilate the entrance. A clue as to the nature of the opening is provided by the structural repeat. The inner and outer sets of coiled coils (H7/H8 and H3/H4, respectively) have similar sequences, which means that they could in principle make similar interhelical interactions. The two sets of coiled coils differ only by small changes in superhelical twist, as shown in Fig. 2b, where we have superimposed the two structural repeats. Hence, the inner pair could re-pack to become congruent with the outer pair by an economical, untwisting movement. Comparable untwisting motions of coiled coils have been noted in other allosteric proteins²⁸. The proposal shares some similarity with the pore-opening mechanism proposed for the transmembrane helices of the acetylcholine receptor²⁹. Using the same reference frame as the superposition of Fig. 2b, the TolC open state was modelled by replacing the inner set of coiled coils with the outer set (Fig. 5). The uncoiling movement of the inner set of coiled coils could open the tunnel by as much as 30 Å.

We propose that the uncoiling movement is triggered by protein–protein interaction, that is, on recruitment of TolC by the inner membrane translocase. The equatorial domain is one possible recognition site for such interaction. Its strands and helices pack against the inner set of coiled coils, and any change in this relationship, induced by interactions with a partner protein, might activate an allosteric transition in the coiled coils. In the modelled open state, the inner coiled coil loses its contacts with the outer coil (for example, H3/H4 packing against H7/H8, see Fig. 3a), but these could be replaced by contacts with the bound translocase. It is noteworthy that the translocase components interacting with TolC¹ have sequence signatures for a coiled-coil motif. Perhaps in the open complex this coiled-coil domain re-packs against the unwound coiled coils at the proximal end of TolC. As the TolC protomer has approximate twofold symmetry, the open structure would have quasi-sixfold symmetry (Fig. 5), and could match the trimeric or hexameric partner in the inner membrane (it has been shown that the translocase partner interacting with TolC is at least trimeric¹).

The structure of the TolC channel tunnel reveals a mechanism to facilitate the direct passage of substrates across two membranes and the intervening periplasmic space. During transport, TolC is recruited by an energized inner membrane translocase in response to substrate engagement, providing substrate specificity and regulated access to the tunnel. This series of events establishes a continuous conduit that transiently connects the cell cytosol to the external environment through a completely proteinaceous machinery. This may have relevance beyond prokaryotic cell function, for example in the direct import of proteins across the two membranes of mitochondria³⁰. The sequence similarity of TolC family members suggests that the principal structural features are

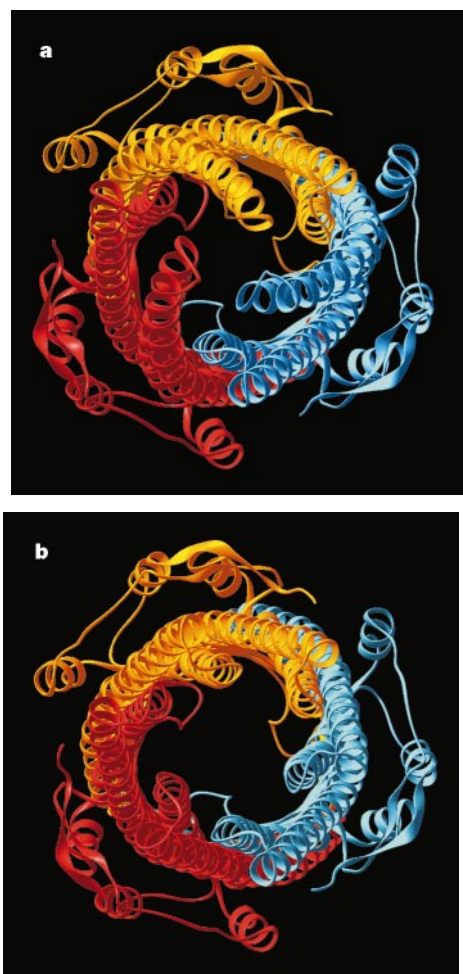


Figure 5 Exterior view of the proximal end of the α -helical barrel, approximately down the threefold symmetry axis. **a**, Crystal structure highlighting the coiled coils closing the proximal end of the tunnel. **b**, ‘Open-state’ model illustrating how the channel may be opened.

conserved, and that the allosteric mechanism proposed may be general to bacterial efflux pumps effecting transport of proteins, antibiotics and other molecules. □

Methods

Protein expression, purification and crystallization

The TolC protein was overexpressed in *E. coli* strain BL21(DE3), purified following detergent extraction as described¹² and treated with V8 protease (500 units per 30 mg protein, 24 h at 30 °C). This cleaved only once, removing the C-terminal 43 residues (a recombinant truncated TolC lacking these 43 residues retained wild-type TolC protein export and bile-salt resistance functions when expressed in *E. coli*). The cleaved protein was re-purified by anion-exchange (Q sepharose). Protein crystals were grown by vapour diffusion from hanging drops at 25 °C. The concentrations of reagents in the drops were a 0.6% detergent mixture of (*n*-dodecyl- β -D-glucopyranoside, *n*-hexyl- β -D-glucopyranoside, *n*-heptyl- β -D-glucopyranoside and *n*-octyl- β -D-glucopyranoside), 1.5% 1,2,3-heptanetriol, 7% polyethylene glycol 2000 monomethyl ether, 10% polyethylene glycol 400, 10 mM NaCl, 20 mM MgCl₂, 20 mM Tris, pH 7.4, and a protein concentration of 10–15 mg ml⁻¹. The drops were equilibrated against 12.5% polyethylene glycol 2000 monomethyl ether, 400 mM NaCl, 20 mM Tris, pH 7.4. Crystals usually appeared within 24–48 h. Initial screens with native TolC for heavy-atom derivatives were unsuccessful; however it was found that the addition of 0.5 mM potassium gold cyanide to the droplets slowed down nucleation and crystal growth, resulting in larger and much more strongly diffracting crystals. There was no evidence of bound gold in the crystals, and gold cyanide was routinely added to all subsequent crystallizations. Crystals of native TolC and derivatives were stabilized in 7% polyethylene glycol 2000 monomethyl ether, 10% polyethylene glycol 200, 15% polyethylene glycol 400, 1.5% 1,2,3-heptanetriol, 0.4% detergent mixture, 0.25 M NaCl, 20 mM MgCl₂, 20 mM Tris pH 7.4 and rapidly frozen at 100K for storage and data collection.

Data collection and structure determination

A series of 10 Ser→Cys point mutants were prepared and pretreated with a variety of mercury compounds before crystallization. Of those that gave usable crystals, only one (S402C) treated with mercury ethyl acetate showed some degree of derivatization. The crystals diffracted weakly and, although 4.0 Å data were collected on station BM14 at the ESRF (Grenoble), near the mercury LIII-edge, the data were useful only to 5.0 Å. Peaks were readily apparent in an anomalous Patterson map, corresponding to three equidistant mercury atoms per asymmetric unit, but the occupancy was very low (~0.15 per site) and the derivative contributed little to the overall phasing power. It was, however, useful at early stages of model building for corroborating the trace and determining the non-crystallographic symmetry operators.

A SeMet derivative was prepared after re-transforming into the met⁻ *E. coli* B834(DE3). Initial MAD data collections were unsuccessful, and we noted that the fluorescence spectra of the SeMet crystals were broad and lacked a characteristic 'white line' at the absorption peak, suggesting heterogeneity in the oxidation state of the selenium. Oxidation of the SeMet residues in TolC by pretreatment of the protein with 0.1% hydrogen peroxide before crystallization resulted in a sharpened fluorescence spectrum and significantly enhanced the amplitude of the fluorescence signal¹³. MAD data were collected from the oxidized SeMet TolC crystals at station BM14 at ESRF and station ID19 at the APS (Chicago) to 3.0 Å and 2.1 Å, respectively. The data were processed with HKL2000 (ref. 31).

Fourteen of the expected fifteen selenium sites were found from the 3.0 Å MAD data using SOLVE³². The final site was located from difference Fourier maps. The selenium parameters were refined and phases calculated using SHARP³³. Phases were improved by density modification, including threefold averaging through matrices defined by the heavy-metal sites, using DM^{34,35}. The initial figure of merit was 0.84 at 3.0 Å. The map was of sufficient quality to trace the entire backbone and assign side chains using the Se and Hg sites as landmarks. Subsequently, the model resolution was extended to 2.1 Å against data collected at the APS. The model was refined with CNS³⁶, applying strict non-crystallographic symmetry constraints, and improved using wARP³⁷ to model solvent. The final stages of refinement were carried out using BUSTER³⁸, which modifies the phases by a maximum likelihood algorithm. The resulting maps were substantially improved and helped to improve the clarity of the density in the poorly ordered loop regions of the β -barrel domain. The non-crystallographic symmetry restraints were relaxed during these later stages and the final cycle was carried out with no restraints. We observe no clear indication of localized lipid or detergent around TolC. The model was also refined against the 2.5 Å native data (collected at station 9.6, Daresbury). The two refined structures show that treatment with peroxide did not cause any detectable structural changes in the protein.

Received 14 March; accepted 4 May 2000.

1. Thanabalu, T., Koronakis, E., Hughes, C. & Koronakis, V. Substrate-induced assembly of a contiguous channel for protein export from *E. coli*: reversible bridging of an inner-membrane translocase to an outer membrane exit pore. *EMBO J.* **17**, 6487–6496 (1998).
2. Paulsen, I. T., Park, J. H., Choi, P. S. & Saier, M. H. A family of Gram-negative bacterial outer membrane factors that function in the export of proteins, carbohydrates, drugs and heavy metals. *FEMS Microbiol. Lett.* **156**, 1–8 (1997).
3. Koronakis, V., Koronakis, E. & Hughes, C. Isolation and characterisation of the C-terminal signal directing export of *E. coli* hemolysin across both bacterial membranes. *EMBO J.* **8**, 595–605 (1989).
4. Koronakis, V., Hughes, C. & Koronakis, E. Energetically distinct early and late stages of HlyB/HlyD-dependent secretion across both *Escherichia coli* membranes. *EMBO J.* **10**, 3263–3272 (1991).
5. Duong, F., Eichler, J., Price, A., Leonard, M. R. & Wickner, W. Biogenesis of the Gram-negative bacterial envelope. *Cell* **91**, 567–573 (1997).

6. Glaser, P., Sakamoto, H., Bellalou, J., Ullmann, A. & Danchin, A. Secretion of cyclolysin, the calmodulin-sensitive adenylate cyclase-hemolysin bifunctional protein of *Bordetella pertussis*. *EMBO J.* **7**, 3997–4004 (1988).
7. Koronakis, V. & Hughes, C. Bacterial signal peptide-independent protein export: HlyB-directed secretion of hemolysin. *Sem. Cell Biol.* **4**, 7–16 (1993).
8. Gilson, L., Mahanty, H. K. & Kolter, R. Genetic analysis of an MDR-like export system: the secretion of colicin V. *EMBO J.* **9**, 3875–3894 (1990).
9. Nikaïdo, H. Multidrug efflux pumps of Gram-negative bacteria. *J. Bacteriol.* **178**, 5853–5859 (1996).
10. Zgurskaya, H. I. & Nikaïdo, H. Bypassing the periplasm: reconstitution of the acrA/B multidrug efflux pump of *Escherichia coli*. *Proc. Natl. Acad. Sci. USA* **96**, 7190–7195 (1999).
11. Stone, B. J. & Miller, V. L. *Salmonella enteritidis* has a homolog of TolC that is required for virulence in BALB/C mice. *Mol. Microbiol.* **17**, 701–712 (1995).
12. Koronakis, V., Li, J., Koronakis, E. & Stauffer, K. Structure of TolC, the outer-membrane component of the bacterial type I efflux system, derived from two-dimensional crystals. *Mol. Microbiol.* **23**, 617–626 (1997).
13. Sharff, A. J., Koronakis, E., Luisi, B. & Koronakis, V. Oxidation of selenomethionine: Some MADness in the method! *Acta Crystallogr. D* **56**, 785–788 (2000).
14. Benz, R., Maier, E. & Gentshev, I. TolC of *Escherichia coli* functions as an outer membrane channel. *Zentralbl. Bakteriol.* **278**, 187–196 (1993).
15. Lupas, A. Predicting coiled-coil regions in proteins. *Curr. Opin. Struct. Biol.* **7**, 388–393 (1997).
16. Johnson, J. M. & Church, G. M. Alignment and structure prediction of divergent protein families: periplasmic and outer membrane proteins of bacterial efflux pumps. *J. Mol. Biol.* **287**, 695–715 (1999).
17. Pautsch, A. & Schulz, G. E. Structure of the outer membrane protein A transmembrane domain. *Nature Struct. Biol.* **5**, 1013–1017 (1998).
18. Schirmer, T. et al. Structural basis for sugar translocation through maltoporin channels at 3.1 Å resolution. *Science* **267**, 512–514 (1995).
19. Cowan, S. W. et al. Crystal structures explain functional properties of two *E. coli* porins. *Nature* **358**, 727–733 (1992).
20. Kreusch, A. et al. Structure of the membrane channel porin from *Rhodospseudomonas blastica* at 2.0 Å resolution. *Protein Sci.* **3**, 58–63 (1994).
21. Snijder, H. J. et al. Structural evidence for dimerization-regulated activation of an integral membrane phospholipase. *Nature* **401**, 717–721 (1999).
22. Buchanan, S. K. et al. Crystal structure of the outer membrane active transporter FepA from *Escherichia coli*. *Nature Struct. Biol.* **6**, 56–63 (1999).
23. Locher, K. P. et al. Transmembrane signalling across the ligand-gated FhuA receptor: crystal structures of free and ferrichrome-bound states reveal allosteric changes. *Cell* **95**, 771–778. (1998).
24. Ferguson, A. D. et al. Siderophore-mediated iron transport: Crystal structure of FhuA with bound lipopolysaccharide. *Science* **282**, 2215–2220 (1998).
25. Schulz, G. E. Porins: general to specific, native to engineered passive pores. *Curr. Opin. Struct. Biol.* **6**, 485–490 (1996).
26. Seo, J. & Cohen, C. Pitch diversity in α -helical coiled coils. *Proteins Struct. Funct. Genet.* **15**, 223–234 (1993).
27. Crick, F. H. C. The packing of α -helices: simple coiled coils. *Acta Crystallogr. B* **6**, 689–697 (1953).
28. Oas, T. G. & Endow, S. A. Springs and hinges: dynamic coiled coils and discontinuities. *Trends Biochem. Sci.* **19**, 51–54 (1994).
29. Unwin, N. Acetylcholine receptor channel imaged in the open state. *Nature* **373**, 37–43 (1995).
30. Schatz, G. & Dobberstein, B. Common principles of protein translocation across membranes. *Science* **271**, 1519–1526 (1996).
31. Otwinowski, Z. & Minor, W. Processing of X-ray diffraction data collected in oscillation mode. *Methods Enzymol.* **276**, 307–326 (1997).
32. Terwilliger, T. C. & Berendzen, J. Automated structure solution for MIR and MAD. *Acta Crystallogr. D* **55**, 849–861 (1999).
33. de la Fortelle, E. & Bricogne, G. Maximum-likelihood heavy-atom parameter refinement in the MIR and MAD methods. *Methods Enzymol.* **276**, 472–494 (1997).
34. Collaborative Computer Project No. 4. The CCP4 suite: programs for protein crystallography. *Acta Crystallogr. D* **50**, 760–763 (1994).
35. Cowtan, K. in *Joint CCP4 and ESF-EACBM Newsletter on Protein Crystallography* Vol. 31 34–38 (Daresbury Laboratory, Daresbury, UK, 1994).
36. Brünger, A. T. et al. Crystallography and NMR system: a new software suite for macromolecular structure determination. *Acta Crystallogr. D* **54**, 905–921 (1998).
37. Perrakis, A., Sixma, T. K., Wilson, K. S. & Lamzin, V. S. wARP: improvement and extension of crystallographic phases by weighted averaging of multiple refined dummy atomic models. *Acta Crystallogr. D* **53**, 448–455 (1997).
38. Bricogne, G. Direct phase determination by entropy maximization and likelihood ranking: status report and perspectives. *Acta Crystallogr. D* **49**, 37–60 (1993).
39. Carson, M. Ribbons. *Methods Enzymol.* **277**, 493–505 (1997).
40. Nicholls, A., Sharp, K. A. & Honig, B. Protein folding and association: insights from the interfacial and thermodynamic properties of hydrocarbons. *Proteins Struct. Funct. Genet.* **11**, 281–296 (1991).

Supplementary information is available on Nature's World-Wide Web site (<http://www.nature.com>) or as paper copy from the London editorial office of Nature.

Acknowledgements

We thank A. Thompson, K. Henderson, N. Duke, A. Joachimski, Z. Otwinowski, W. Minor, K. Phillips, M. Symmons and F. von Delft for help during data collection and discussions; C. Calladine, M. Perutz, J. Li and C. Andersen for discussions; and G. Bricogne and P. Roversi for help with the BUSTER program. We acknowledge support for EU facility access for data collection at DESY (Hamburg) and ESRF (Grenoble). This work is supported by a Medical Research Council Programme grant (to V.K. and C.H.). A.S. and B.L. are supported by the Wellcome Trust.

Correspondence and requests for materials should be addressed to V.K. (e-mail: vk103@mole.bio.cam.ac.uk). Coordinates have been deposited in the RCSB protein data bank under accession code 1EK9.